EDGE ARTICLE

Check for updates

Multi-functional nitrile-based electrolyte additives enable stable lithium metal batteries with high-voltage nickel-rich cathodes†

Shu Yang,‡[a] Haonan Huang,‡[b] Hailin Shen,[c] Mengyuan Zhou,[a] Liang Yuan,[a] Yunyun Gao,[a] Jinlei Zhang,[a] Yike Wei,[a] Changchun Ye,*[bd] Weishan Li [ID][b] and Zhenghui Pan [ID] *[a]

A rechargeable lithium (Li) metal anode combined with a high-voltage nickel-rich layered cathode has been considered a promising combination for high-energy Li metal batteries (LMBs). However, they usually suffer from insufficient cycling life because of the unstable electrochemical stability of both electrodes. In this work, we report an advanced multi-functional additive, 1,3,6-hexanetricarbonitrile (HTCN), in a conventional carbonate-based electrolyte. This rationally designed electrolyte formation generates an ideal cathode electrolyte interphase (CEI) for $LiNi_{0.8}Co_{0.1}Mn_{0.1}O_2$ (NCM811) and a solid electrolyte interphase (SEI) for Li metal, successfully realizing stable ion transport kinetics. Then, theoretical calculations, physical characterization and electrochemical tests confirm that HTCN is more easily adsorbed on the NCM811 surface where it is oxidized to construct a stable CEI film involving the detachment of the CN group in a linear chain. Simultaneously, HTCN shows a more negative electron affinity and is easier to reduce, constructing a robust SEI film resulting from the detachment of the CN group in the side chain. Consequently, the assembled 50 μm-thin NCM811//Li (9.0 mg cm^{-2} of mass loading) delivers a desired energy density of ~330 W h kg^{-1} at the cell level and an excellent cycling stability of 120 cycles with 88% capacity retention at 1C.

1. Introduction

Lithium (Li) metal is considered to be the "holy grail" of the anode for next-generation energy storage batteries due to its ultra-high theoretical specific capacity (3860 mA h g^{-1}, almost ten times that of commercial graphite) and ultra-low redox potential (~3.04 V *vs.* the standard hydrogen electrode, SHE).[1-6] Rechargeable Li metal batteries (LMBs) produced with various cathode materials, especially the high-voltage $LiNi_{0.8}Co_{0.1}Mn_{0.1}O_2$ (NCM811) cathode, have recently received widespread attention.[7-10] However, the high reactivities of Li and NCM811 electrodes with conventional carbonate electrolytes result in various non-negligible problems,[11-13] which hinder the practical application of high-energy NCM811//Li batteries. The main

issues faced by nickel-rich NCM811 cathodes are structural damage of the active material resulting from the uneven cathode electrolyte interface (CEI) film and corrosion by hydrogen fluoride (HF) acid.[4,14-18] On the side of the Li metal anode, the fundamental problem is the instability of the solid electrolyte interface (SEI),[19,20] which leads to uneven current distribution on the Li surface and thus triggers the dendrite growth and the accumulation of dead Li.[21-24] Therefore, it is critical to synchronously enhance the interfacial stability of the NCM811 cathode and Li metal anode required for high-energy LMBs.

Many functional electrolytes from the perspectives of designing solvents, salts and additives at the molecular level have been developed.[25-30] After in-depth consideration of cost and the process, it is a promising method to construct thin and uniform CEI/SEI films to separate electrolytes and electrodes by adding additives known as "vitamins" of batteries.[31-34] Moreover, the development of multifunctional additives that not only form CEI/SEI films but also inhibit the generation of HF has tremendous application advantages.[35,36] Therefore, it is essential to develop electrolyte additives with multiple functions. Nitrile additives are widely used in high-voltage Li-ion batteries (LIBs). The prevailing mechanism is that nitriles can effectively coordinate with transition metal ions and participate in the formation of the CEI/SEI films,[37-39] but they have rarely been

[a]*School of Materials Science and Engineering, Tongji University, Shanghai 201804, China. E-mail: zhenghuipan@tongji.edu.cn*

[b]*School of Chemistry, South China Normal University, Guangzhou 510006, China. E-mail: esyecc@mail.scut.edu.cn*

[c]*School of Chemical Engineering and Materials, Changzhou Institute of Technology, Changzhou, China*

[d]*School of Physics and Optoelectronics, South China University of Technology, Guangzhou 510006, China*

† Electronic supplementary information (ESI) available. See DOI: https://doi.org/10.1039/d4sc08045a

‡ S. Yang and H. Huang contributed equally to this work.

used for LMBs because of their strong reducing activity.[40–42] For example, even with ultrahigh concentration salt (10 M) in acetonitrile (AN) solvent, the Coulombic Efficiency (CE) of a Li// Cu cell is still poor at ≈14%.[8] Therefore, selecting a nitrile additive with suitable reductive activity so that it decomposes to form CEI/SEI films but does not decompose excessively is vital for developing high-energy LMBs.

In this work, a novel multi-functional nitrile additive, 1,3,6-hexanetricarbonitrile (HTCN) with linear and side-chain CN groups, is proposed for improving the electrochemical performance of the high-voltage NCM811 cathode and Li metal anode. The underlying film-forming mechanism was thoroughly studied by electrochemical characterization and theoretical calculations. The results show that HTCN can preferentially be adsorbed and oxidized to form a stable CEI rich in CN-containing species, involving the detachment of the CN group in the linear chain and the repolymerization of F^-, which significantly inhibits the electron exchange between the electrolyte and NCM811 cathode (Fig. 1). Meanwhile, lower electron affinity energy drives the preferential reduction of the HTCN additive resulting from the detachment of the CN group in the side chain and the participation of PF_6^- anions in the polymerization, followed by forming a SEI film rich in crosslinked polymers, which suppresses the electrolyte decomposition and dendrite growth. Besides, the stronger binding intensity between HTCN and PF_6^- than that of solvents efficiently prevents the generation of harmful HF. Based on the above advantages, both NCM811//Li and Li//Li half-cells present stable cycle stability. More significantly, a desired energy density of 330 W h kg^{-1} at the cell level and an excellent cycling stability of 120 cycles with 88% capacity retention at 1C for 50 μm-thin Li// NCM811 (9.0 mg cm^{-2} of mass loading) full batteries are achieved.

2. Experimental section

2.1 Sample preparation

The baseline electrolyte used in this work is 1 M LiPF$_6$ (>99.8%) dissolved in ethylene carbonate (EC)/dimethyl carbonate (DMC) (30/70 wt%) (Guangzhou Tianci Materials Technology Co. Ltd, China). 1,3,6-hexanetricarbonitrile (HTCN, Aladdin, >99.0%) and adiponitrile (ADN, Aladdin, >99.0%) were added to the baseline electrolyte to obtain the electrolyte containing a single additive.

To prepare the NCM811 cathode, 80 wt% NCM811 powder (Ningbo Jinhe New Materials Co., Ltd), 10 wt% acetylene black (AB, Shenzhen Kejing Star Technology Co., Ltd) and 10 wt% polyvinylidene fluoride (PVDF, Shenzhen Kejing Star Technology Co., Ltd) were mixed in N-methylpyrrolidone (NMP) solvent to form an NCM811 slurry. NCM811 was developed by coating slurry with different NCM811 contents on aluminium foil after drying at 80 °C for one hour and at 120 °C for 12 h under vacuum. The dried NCM811 electrodes were obtained and were then cut into round pieces with a diameter of 12 mm and transferred to a glove box (Mbraum Unilab, Germany), where water and oxygen contents were strictly controlled below 0.1 ppm. The thick-Li foil in L-NCM811//Li has a diameter of 16 mm and a thickness of 0.5 mm. The H-NCM811//Li full cells were assembled with an NCM811 cathode and Li foil anode with a diameter of 13 mm and a thickness of 50 μm. The CR2025-type NCM811//Li and Li//Li coin batteries were assembled in a glove box with Celgard 2325 separators (diameter = 18 mm, thickness = 20 μm) containing 60 μL of electrolyte. The preparation of the electrolyte and the assembly/ disassembly of the batteries are carried out in a glove box.

2.2 Electrochemical measurement

The cycling stability of cells was tested on a battery tester (LAND CT2001A, China). NCM811//Li cells were charged/discharged at 0.2C (1C = 200 mA h g^{-1}) for the initial 3 cycles and at 1C for the subsequent cycles between 3.0 and 4.35 V with a constant voltage at 4.35 V for 10 minutes. The rate performance of L-NCM811//Li half cells was tested by discharging at 0.2C, 0.5C, 1C, 3C, 5C, 7C and 10C, respectively. The current density and capacity density of the Li//Li symmetric battery are 1 mA cm^{-2} and 1 mA h cm^{-2}, respectively.

For the self-discharge test, L-NCM811//Li coin cells were charged to 4.35 V at 1C and then left for 30 days to record the potential variation after three initial cycles at 0.2C between 3
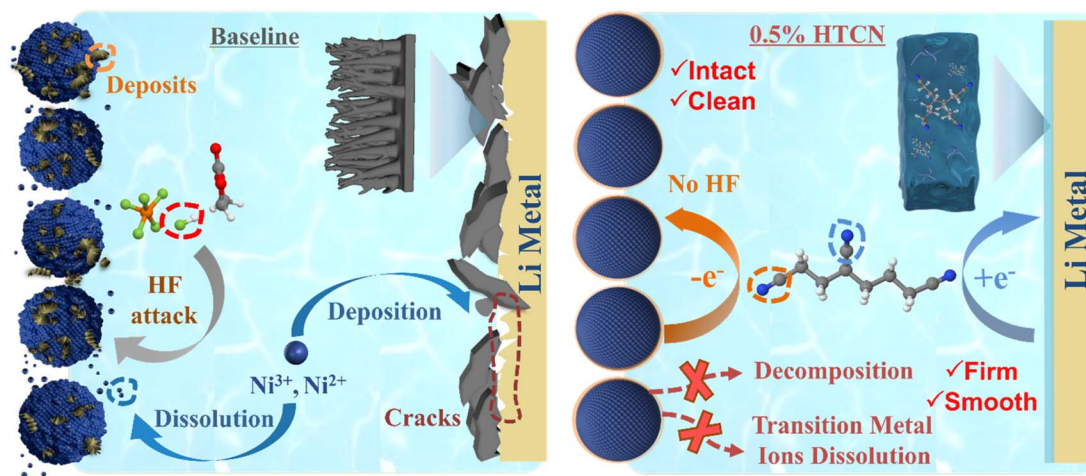

Fig. 1 Schematic illustration of the underlying mechanisms of baseline and HTCN-containing electrolytes.

and 4.35 V. Linear sweep voltammetry (LSV) was carried out on a Solartron 1480 (England) to test the oxidation stability of the electrolyte. The V-type cells were assembled and scanned from the open circuit potential (OCP) to 5 V with a scanning rate of 0.1 mV s^{-1}. Electrochemical impedance spectroscopy (EIS) was carried out using a PGSTAT-30 (Switzerland). The cells to be tested were all in a discharge state, with a frequency range from 100 kHz to 0.005 Hz at a voltage amplitude of 5 mV.

2.3 Physical characterization

The contact angle between the separator and various electrolytes was tested on a contact angle system (JC2000C, China) and the ionic conductivity of electrolytes was measured on an 856 Conductivity Module (Sweden) at room temperature. Before characterization, the cycled cells were disassembled and the recovered electrodes were soaked in DMC for 5 minutes, washed 3 times, and then dried naturally in a glove box for further use. Scanning electron microscopy (SEM, FEI-quanta 250, America) and transmission electron microscopy (TEM, JEM-2100HR, Japan) were used to observe the morphologies of the electrode surfaces and the interfacial films formed on the NCM811 cathode. X-ray diffraction patterns (XRD, Rigaku Ultima IV, Japan) of NCM811 electrodes were obtained by using monochromatic Cu Kα radiation between 10° and 90° with a scanning rate of 5° min^{-1}. The chemical compositions and contents of each component in the interfacial films were anatomized by X-ray photoelectron spectroscopy (XPS, AXIS SUPRA, Japan). Nuclear magnetic resonance (NMR) analysis was performed on a Bruker AVANCE NEO spectrometer (Bruker, Germany). Fourier transform infrared (FTIR) spectroscopy was performed on a Bruker Tensor 27 (Germany). The contents of transition metals (TMs) deposited on the Li anodes were determined by inductively coupled plasma atomic emission spectrometer measurement (ICP-AES, Optima 8300, America). For Li anodes, the cycled Li anodes were fully dissolved in 4 wt% HNO$_3$ solution and then diluted to 25 mL with deionized water to obtain a sample solution.

2.4 Theoretical calculation

All the calculations involved in this work were performed with the Gaussian 16 package. The molecular structures of the solvents and additives in the electrolyte were optimized based on density functional theory (DFT). The oxidation and reduction activities of each molecule and cluster, as well as the binding energies between each molecule and PF$_6^-$, Ni^{3+} and Ni^{2+} were calculated according to the optimized geometric structures using the B3LYP/6-311++G(d) level basis set. A polarized continuum model (PCM) with acetone (dielectric constant = 20.5) was adopted. NBO charge distributions of the HTCN additive after reduction were analyzed to deduce the intermediates. The vibrational frequencies and intrinsic reaction coordinate (IRC) analysis were used to ensure that the sought transition state was the saddle point for the lowest energy path connecting the reactants and products.

3. Results and discussion

3.1 Effect of the HTCN additive on the electrochemical performance of the NCM811 cathode

The L-NCM811//Li half cells were first assembled using the NCM811 cathode with 1.5 mg cm^{-2} mass loading and a 500 μm Li film anode to verify the effect of the HTCN additive. As expected, cyclic testing shows rapid capacity decay with a capacity retention rate of 51% after 100 cycles in baseline electrolyte (Fig. 2a), resulting from poor compatibility and parasitic side reactions between the NCM811 cathode and electrolyte. In contrast, the cycle stability of the L-NCM811//Li cell in HTCN-containing electrolytes is significantly improved with a specific capacity of 167.2 mA h g^{-1} (a capacity retention rate of 84%) after 100 cycles. Furthermore, the rate capability can be largely enhanced with the application of the HTCN additive, with a discharge-specific capacity of up to 10C (Fig. 2b). These indicate that the interface film derived from HTCN-containing electrolyte increases the compatibility of the NCM811 cathode and carbonate electrolyte, although its wettability and conductivity are slightly reduced (Fig. S1 and S2†). TEM and SEM images of the cycled NCM811 cathodes show some irregular loose deposition products on the surface of the NCM811 nanoparticle after 3 cycles in the baseline electrolyte (Fig. 2c), leading to continuous electron exchange between the NCM811 primary particles and solvent. Therefore, the electrolyte decomposition products on the surface of materials continue to accumulate with the cycling (Fig. 2e and g), eventually leading to the destruction and collapse of the material structure. In contrast, an ideal CEI film is formed on the surface of NCM811 after 3 cycles in the HTCN-containing electrolytes (Fig. 2d), which still has a smooth surface (Fig. 2f) and retains its complete structure after 100 cycles (Fig. 2h). XRD characterization was used to analyze the structural changes of the NCM811 electrode in baseline and HTCN-containing electrolytes (Fig. S3†). The α-NaFeO$_2$ layered structure of the NCM811 material almost disappears in the baseline electrolyte.[43,44] Specifically, the (003) and (108) peaks shift to a smaller angle while the (101) peak shifts to a larger angle, which presents the variation of lattice constants and the structural transformation of the NCM811 cathode from the layer phase to the spinel phase (Fig. S4†), indicating that the structure is severely damaged in baseline electrolyte. Compared with it, the good splitting of the (108)/(110) peaks shows that great layered characteristics were maintained in HTCN-containing electrolyte, indicating that the HTCN additive can effectively support the NCM811 electrode to maintain good stability.[45] These results indicate that the HTCN additive can effectively suppress electrode/electrolyte interfacial side reactions, including the decomposition of the electrolyte and the dissolution of transition metals. The impedances of the L-NCM811//Li cell after 3 and 100 cycles were measured and fitted with an equivalent circuit to further confirm the effect of the HTCN additive on the interface stability (Fig. S5†). Initially, there is no significant difference between baseline and HTCN-containing electrolytes after activation at 0.2C for 3 cycles. As the cycle progresses, the overall impedance of the battery in the
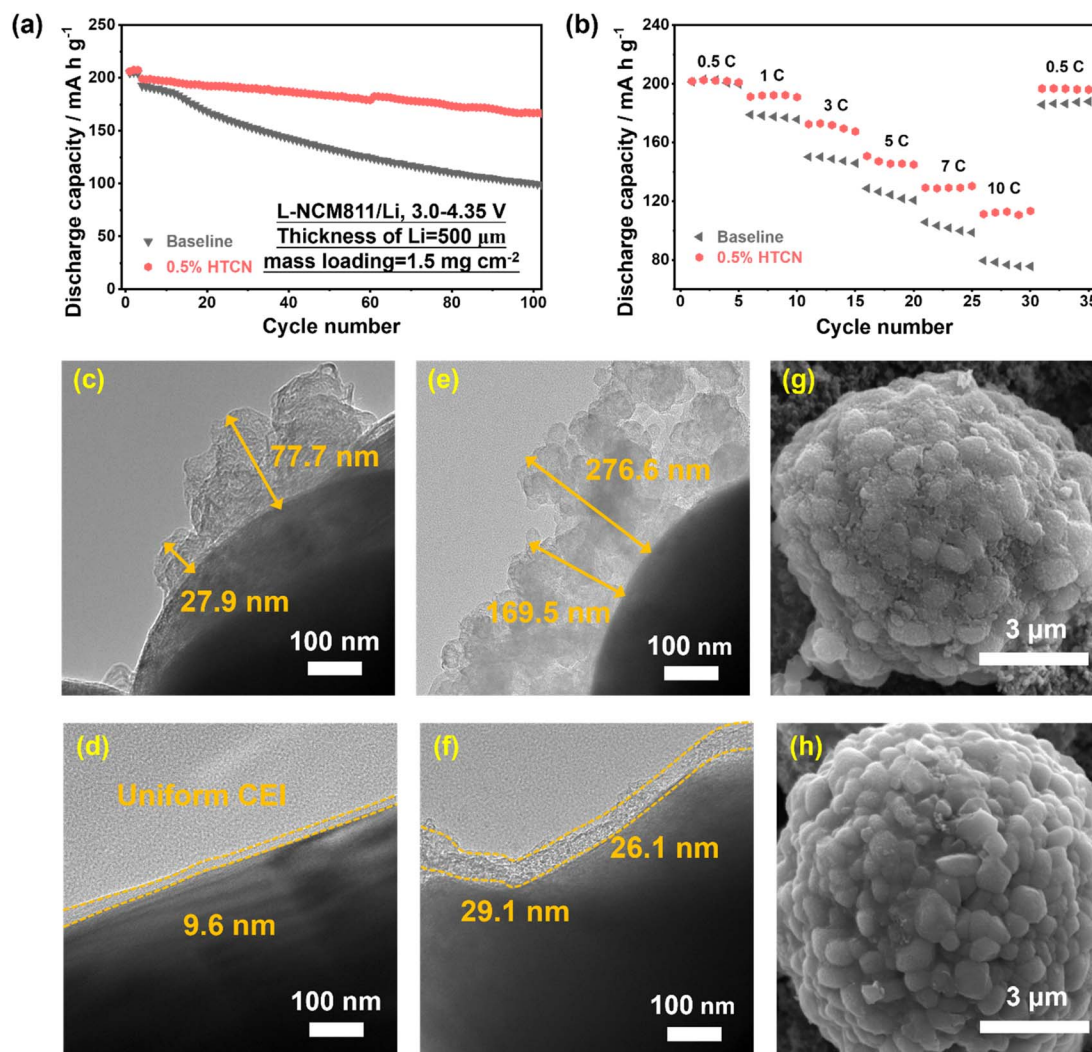
Fig. 2 (a) Cycling stability of L–NCM811//Li cells in various electrolytes at 0.2C for the initial three cycles and 1C for the subsequent 100 cycles. (b) Rate capability for L–NCM811//Li cells in various electrolytes. TEM and SEM images of NCM811 electrodes recovered from L–NCM811//Li cells after (c) 3 cycles and (e and g) 100 cycles in baseline electrolyte. TEM and SEM images of NCM811 electrodes recovered from L–NCM811//Li cells after (d) 3 cycles and (f and h) 100 cycles in HTCN-containing electrolyte.

baseline electrolyte increases significantly due to more electrolyte decomposition products and the fracture of electrode materials (Fig. S5b and d†). In contrast, the battery in HTCN-containing electrolytes maintains a stable impedance during the cycle (Fig. S5c and e†), suggesting its ability to stabilize the NCM811/electrolyte interface.

3.2 Revealing the underlying mechanism of the HTCN additive on the NCM811 cathode

To investigate the oxidation activities of the solvent and additive in the HTCN-containing electrolytes, the ionization energies of each component and the complexed PF_6^- clusters were calculated based on density functional theory (DFT). The results show that HTCN has slightly lower oxidation activity than that of solvent molecules, both as single molecules and clusters (Fig. 3a and S6†). In addition to the oxidation activity, the adsorption strength on the electrode surface also greatly affects the preferential oxidation order of the electrolyte components. DFT calculations demonstrate that HTCN has strong binding abilities both with Ni^{2+} and Ni^{3+} ions, which means that HTCN easily aggregates on the surface of the NCM811 cathode (Fig. 3b and S7†). Considering the slightly different theoretical oxidation activities, we infer that the adsorption capacity is decisive and HTCN has the potential for preferential oxidation. Moreover, HTCN presents a stronger binding ability with PF_6^- than EC and DMC, which is beneficial to inhibiting the thermal decomposition of PF_6^- and reducing the presence of harmful HF (Fig. S8†).

The linear sweep voltammetry (LSV) test on the Pt electrode was used to verify the oxidizing activity of various electrolytes. The current of the baseline electrolyte starts to increase sharply when the electrode potential is scanned to 4.2 V (Fig. 3c), indicating that the electrolyte decomposes violently at high voltage. However, an earlier response current at around 3.75 V is
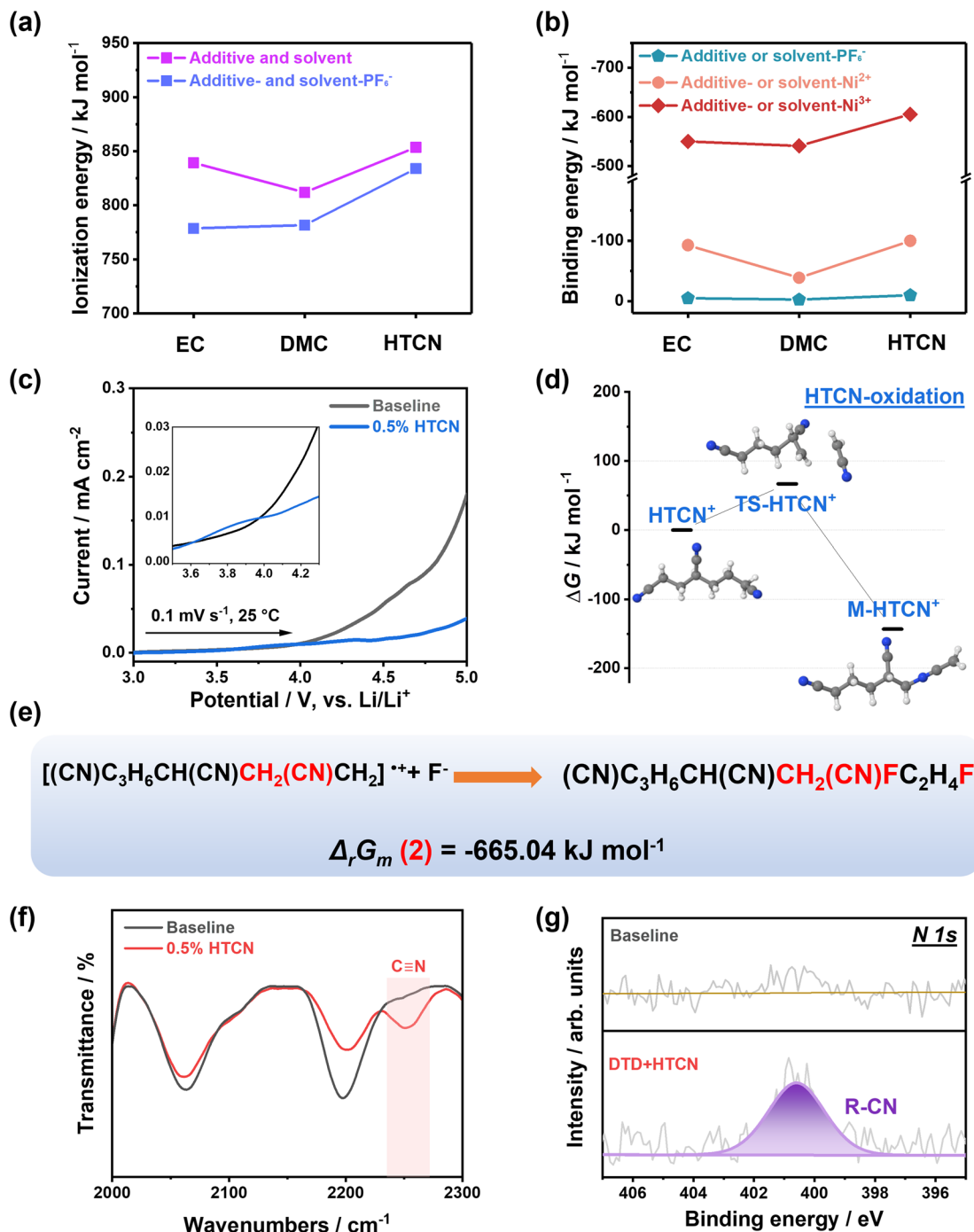
Fig. 3 (a) Calculated adiabatic ionization energies (AIE, kJ mol^{-1}) of EC, DMC and HTCN before and after combining with PF$_6^-$. (b) Calculated binding energies (E_b, kJ mol^{-1}) between EC, DMC, and HTCN and PF$_6^-$, Ni^{2+} and Ni^{3+}. (c) LSV of baseline and HTCN-containing electrolytes on the Pt electrode from OCP to 5.0 V at a scan rate of 0.1 mV s^{-1}. (d and e) Possible oxidation reaction paths of the HTCN additive. (f) FTIR and (g) XPS spectra of NCM811 cathodes recovered from L-NCM811//Li cells after 20 cycles in baseline and HTCN-containing electrolytes.

detected in the HTCN-containing electrolyte, which corresponds to the oxidative decomposition of the HTCN additive, inhibiting the subsequent electrolyte decomposition with a lower response current after 4.2 V. To truly simulate the porous material of the electrode, L-NCM811//Li coin cells were assembled to further verify the preferential oxidation of HTCN, where the content of NCM811 active materials was reduced to

weaken the interference of the delithiation current. Similarly, an earlier oxidation current appeared in the HTCN-containing electrolyte compared with the baseline electrolyte, further demonstrating the preferential oxidation of the HTCN additive (Fig. S9†). DFT calculation was used to explore the oxidation paths and possible reaction products of the HTCN additive (Fig. 3d). The oxidized HTCN$^+$ ion breaks off the acetonitrile

group (–CH_2–CN) to obtain a transition state TS-$HTCN^+$, and then the acetonitrile group, in turn, attacks the radical at the other end to obtain the M-$HTCN^+$ radical cation intermediate. The intermediate products as the free radical cations would polymerize with the anions and free radicals in the electrolyte to produce insoluble products covering the surface of the NCM811 cathode to form CEI components. All anions (PF_6^-, F^-, and CN^-, the pathway of CN^- anion generation will be described in detail in the following section) in electrolytes were taken into account to obtain the most advantageous reaction path and reaction product (Fig. S10†). According to the reaction energies of different paths, M-$HTCN^+$ tends to self-polymerize after binding to the F^- anion to get the oxidation product of HTCN, $(CN)C_3H_6CH(CN)CH_2(CN)FC_2H_4F$ (P-$HTCN^+$) (Fig. 3e). CN^- and CH_2CN^- species are detected by time of flight secondary ion mass spectrometry (TOF-SIMS), as shown in Fig. S11,† proving the reliability of the reaction path, which corresponds to the results of FTIR and XPS spectra (Fig. 3f and g).

3.3 Properties of the CEI derived from the HTCN-containing electrolytes on the NCM811 cathode

The composition difference of the CEI constructed on the NCM811 surface by various electrolytes was analyzed by TOF-SIMS and XPS characterization studies. Fig. 4a and b present the content depth profiles of inorganic (LiF_2^- and $Li_2CO_3^-$) and organic (C_2H^- and $LiCOO^-$) species in the CEI, respectively. There are obvious organic carbon-containing species distributed in the CEI derived from baseline electrolytes, indicating a large amount of oxidation of the solvent (Fig. 4c). In sharp contrast, with the addition of the HTCN additive, the intensity of organic species decreases while that of the inorganic species increases (Fig. 4d). Besides, from the contents of each element on the electrode surface (Fig. S12†), it can be seen that the contents of O^-, P^- and F^- (representing electrolyte decomposition products on the electrode surface) decrease in the additive system, while the intensity of C–C/C–H (representing PVDF and AB gradually) increases, demonstrating that the electrolyte decomposition on the electrode surface is inhibited by the
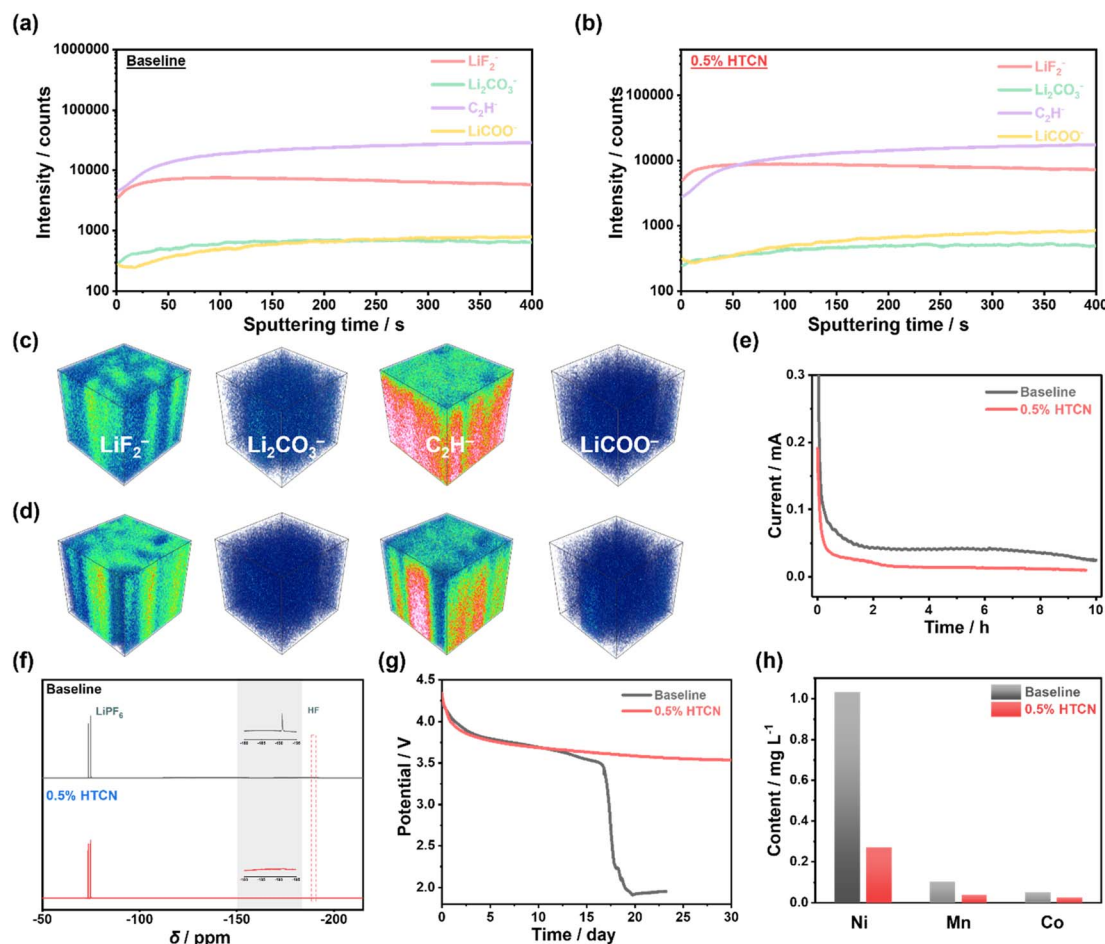

Fig. 4 Intensity sputter profiles of species and corresponding 3D reconstruction distribution mappings on the surface of the NCM811 cathode after cycling in (a and c) baseline and (b and d) HTCN-containing electrolytes measured by TOF-SIMS. (e) Chronoamperometric curves of L-NCM811//Li cells in baseline and HTCN-containing electrolytes at 4.35 V for 20 h after 3 cycles at 0.2C. (f) ^{19}F NMR spectra of baseline and HTCN-containing electrolytes, which were taken from V-type cells after a potential sweep from OCP to 4.35 V at 0.1 mV s^{-1} and constant potential at 4.35 V for 20 h. (g) Self-discharge test of L-NCM811//Li cells for 30 days. (h) Deposition contents of Co, Mn and Ni on the counter Li electrode after 100 cycles.

addition of the HTCN additive, which is consistent with the TOF-SIMS results.

Due to the inevitable presence of residual water, PF_6^- tends to thermally decompose to produce harmful HF,[46] which is more significant during high-temperature storage or high-voltage charging. To further verify the effectiveness of the HTCN additive in suppressing HF, L-NCM811//Li V-type cells were designed and charged at constant voltage at a high potential of 4.35 V. It can be seen that the baseline electrolyte presents a large residual current (Fig. 4e), indicating that the electrolyte decomposition is the most serious. However, the residual current of the HTCN-containing electrolyte decreases significantly, revealing that the HTCN additive is beneficial for inhibiting the oxidative decomposition of the electrolyte. The electrolytes charged at a constant voltage of 4.35 V for 20 h were tested using ^{19}F NMR. The content intensity of HF is almost undetected in the HTCN-containing electrolyte (Fig. 4f), proving the ability of the HTCN additive to eliminate harmful HF. The reason is attributed to the fact that HTCN has the strongest binding ability with PF_6^-, which can trap it and avoid thermal decomposition. Moreover, HTCN can form complexes with F^- and initiate self-polymerization to transfer it to the interfacial film (Fig. 3e). Therefore, HTCN can effectively alleviate the dissolution of transition metal ions caused by HF and retain the structural stability of the cathode material (Fig. 4h). In addition to the cycling performance, HTCN also improves the high-voltage storage performance of L-NCM811, from 16 days in the baseline electrolyte to 30 days in the HTCN-containing electrolyte (Fig. 4g). This is attributed to the HTCN-induced interfacial film that effectively inhibits the electron exchange between the electrolyte and the high-valent transition metal ions (Ni^{4+} and Co^{4+}) in the cathode material, avoiding the oxidative decomposition of the electrolyte and the reduction/dissolution of metal ions.[47,48]

3.4 Effect and underlying mechanism of the HTCN additive on the Li metal anode

Li//Li symmetric cells were assembled to explore the influence of the HTCN additive on the performance of the Li/electrolyte interface. It can be seen that the overpotential of the Li//Li symmetric cell begins to increase rapidly after 150 h in baseline electrolyte (Fig. 5a), with a drastic increase in decomposition products and a passivation layer thickness of up to 217.8 μm (Fig. S13a and b†). In contrast, the overpotential remains stable for 350 h in the HTCN-containing electrolyte without significant polarization, which is attributed to the stable SEI film with a passivation layer of 86.9 μm formed with the participation of the HTCN additive (Fig. S13c and d†). These results indicate a significantly improved compatibility between the carbonate electrolyte and the Li electrode, resulting in minimized consumption of electrolytes and Li dendrite growth. Coulombic efficiency (CE) was used to investigate the cycling behaviour of Li^+ plating/stripping. Although the CE of the cell in the baseline electrolyte is similar to that of the HTCN-containing electrolyte in the initial cycle, the CE drops dramatically after 60 cycles (Fig. 5b). Meanwhile, the voltage

profiles show increasing overpotential (Fig. S14†), suggesting that active Li is consumed due to a deteriorating reaction. In contrast, the HTCN-containing electrolyte shows high CE and good cycling stability (Fig. 5b and S15†), indicating that the HTCN additive inhibits electrolyte decomposition efficiently. The cycled Cu substrate was observed to study the deposition modes of Li^+ and deposition morphologies in different electrolytes. It can be seen that Li^+ is deposited in the form of dendrites in the baseline electrolyte (Fig. S16a†), and the tip with larger polarity will continue to induce Li^+ deposition, promoting the growth of dendrites and subsequently fracture to form dead Li. Consequently, the surface of the Li electrode after 300 h of cycling presents a porous, broken morphology (Fig. S13b†), which can easily cause an internal short circuit, thus causing safety accidents such as thermal runaway of the battery. In contrast, in the HTCN-containing electrolyte, Li^+ is deposited in a disc-type and gradually forms a block shape as the deposited amount grows (Fig. S16d†), which is conducive to inhibiting the parasitic reaction between the electrolyte and the active Li and maintaining long-term cycling stability. Therefore, the electrode surface remains dense and smooth after 300 h of cycling (Fig. S13d†).

Theoretical calculations combined with physical characterization were then applied to explore the underlying mechanism of the HTCN additive on the Li anode. The results show that HTCN exhibits a more negative electron affinity energy (Fig. S17†), suggesting that the HTCN additive can be preferentially reduced compared to the solvent, which is confirmed using the reduction peak around 1.38 V in the LSV (Fig. 5c). XPS and TOF-SIMS results display the present CN-containing species on the surface of Li metal (Fig. S18 and 19†), proving that HTCN is involved in the construction of the SEI. Temperature-dependent electrochemical impedance spectroscopy (EIS) was carried out to calculate corresponding activation energies (E_a) after several cycles to detect the ionic conductivity of the SEI derived from HTCN-containing electrolytes (Fig. 5d and S20†). Compared with the baseline electrode, a lower E_a (48.1 kJ mol^{-1}) for the HTCN-containing electrolyte demonstrates that the SEI containing CN species facilitates fast Li^+ transfer.

The reduction behaviour of HTCN on the surface of the Li electrode was revealed using DFT. The Li^+ (HTCN) clusters in a reduced state passed through the transition state to obtain the intermediates (Fig. 5e), and the NBO charge distribution shows that the intermediate product of HTCN reduction is a radical containing two CN groups and a CN^- anion (Fig. 5f and S21†), of which the CN^- anions spontaneously migrate to the NCM811 cathode surface. The reaction rate is judged from the magnitude of the energy barrier between the reactants and the transition state, where the reduced Li^+ (HTCN) cluster only needs to cross the energy barrier of 38.61 kJ mol^{-1} by passing through the transition state, which indicates that HTCN can easily pass through the transition state to obtain the reaction intermediate. Besides, M-$HTCN^-$ undergoes self-polymerization as a radical intermediate, and P-$HTCN^-$ with a crosslinked structure is formed on the surface of the Li electrode (Fig. 5f). Intensity sputter profiles further characterize the differences in the SEI.
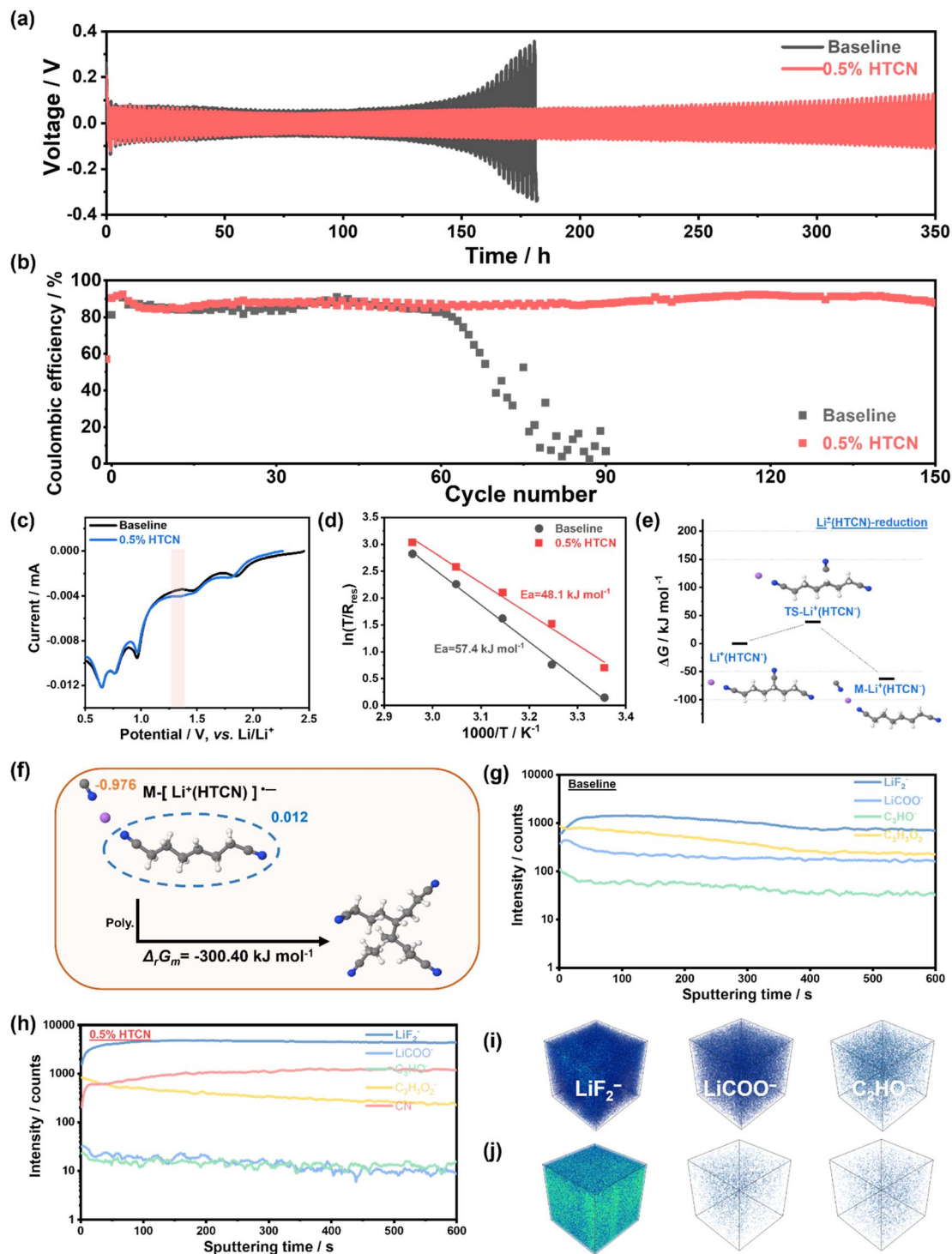
Fig. 5 (a) Cycling stability of Li//Li symmetric cells and (b) CE of Li//Cu asymmetric cells in baseline and HTCN-containing electrolytes. (c) LSV of various electrolytes from OCP to 0.5 V at a scan rate of 1 mV s^{-1}. (d) The activation energy of the SEI derived from the baseline and HTCN-containing electrolytes. (e and f) Possible reduction paths of the HTCN additive. Intensity sputter profiles of species and corresponding 3D reconstruction distribution mappings on the surface of the Li metal anode after cycling in (g and i) baseline and (h and j) HTCN-containing electrolytes measured by TOF-SIMS.

They show that the SEI formed in baseline electrolytes rich in organic species including $LiCOO^-$ and C_2HO^-, while it lacks inorganic species LiF_2^- (Fig. 5g and i), suggesting the severe decomposition of solvents. Fortunately, the amount of LiF_2^-

can be detected in the SEI formed in HTCN-containing electrolyte (Fig. 5h and j), indicating that the HTCN additive promotes the reduction of PF_6^- anions and thus efficiently stabilizes the Li/electrolyte interphase. These results reveal that

the formed 3D network structure combined with inorganic LiF substantially enhances the mechanical strength of the SEI and suppresses the side reactions between the electrolyte and Li metal. In order to verify the specificity of HTCN with the CN group in the side chain, the effect of nitrile without a CN group in the side chain, ADN, on the Li anode was characterized. First, Li//Li symmetric cells were assembled to explore the influence of the ADN additive on the performance of the Li/electrolyte interface. It can be seen that the overpotential of the Li//Li symmetric cell begins to increase rapidly after 80 h in ADN-containing electrolyte (Fig. S22a†), suggesting that the ADN additive is harmful to the cycling stability of Li//Li symmetric cells. Coulombic efficiency (CE) was used further to investigate the cycling behaviour of Li⁺ plating/stripping. Unfortunately, the CE of the cell in ADN-containing electrolyte drops dramatically after 24 cycles (Fig. S22b†), indicating that the interface deteriorates after adding the ADN additive. The above results confirm the validity and specificity of the HTCN additive with the CN group in the side-chain.

3.5 Effect of the HTCN additive on the electrochemical performance of NCM811//Li full cells

H-NCM811/T-Li full batteries were assembled to evaluate the practicability of the HTCN additive on cycle stability, containing high-loaded NCM811 (denoted as H-NCM811, mass loading up to 9 mg cm^{-2}) and a thin Li foil electrode (denoted as T-Li, thickness of 50 μm), which is closer to the LMBs in practical applications. The discharge-specific capacity of the H-NCM811/T-Li full batteries decays rapidly after 75 cycles until 90 cycles to near 0 mA h g^{-1} in the baseline electrolyte (Fig. 6a). Correspondingly, the CE of the battery starts to oscillate in the middle and latter parts of the charge/discharge cycle, suggesting that the violent oxidation/reduction decomposition of the electrolyte occurred on the interfaces of the NCM811 cathode and Li anode. In contrast, the H-NCM811/T-Li cell cycled in the HTCN-containing electrolyte exhibits superior cycle stability (with a capacity retention of 88%, an initial capacity of 200 mA h g^{-1} from 4th cycles corresponding to a desired energy density of ∼330 W h kg^{-1} at the cell level) and stable coulombic efficiency (98.2%), with a discharge specific capacity of 175 mA h g^{-1} after 120 cycles. Charge/discharge curves show that the battery cycled in baseline electrolyte is heavily polarized (the difference between charge and discharge voltage) (Fig. 6b), indicating persistent reactions at the electrode/electrolyte interphase. Fortunately, the HTCN additive can significantly decrease the polarization (Fig. 6c). The batteries were disassembled after 100 cycles and the electrode morphology was observed by SEM. It is demonstrated that the surface of the NCM811 cathode cycled in baseline electrolyte is almost covered by the decomposition
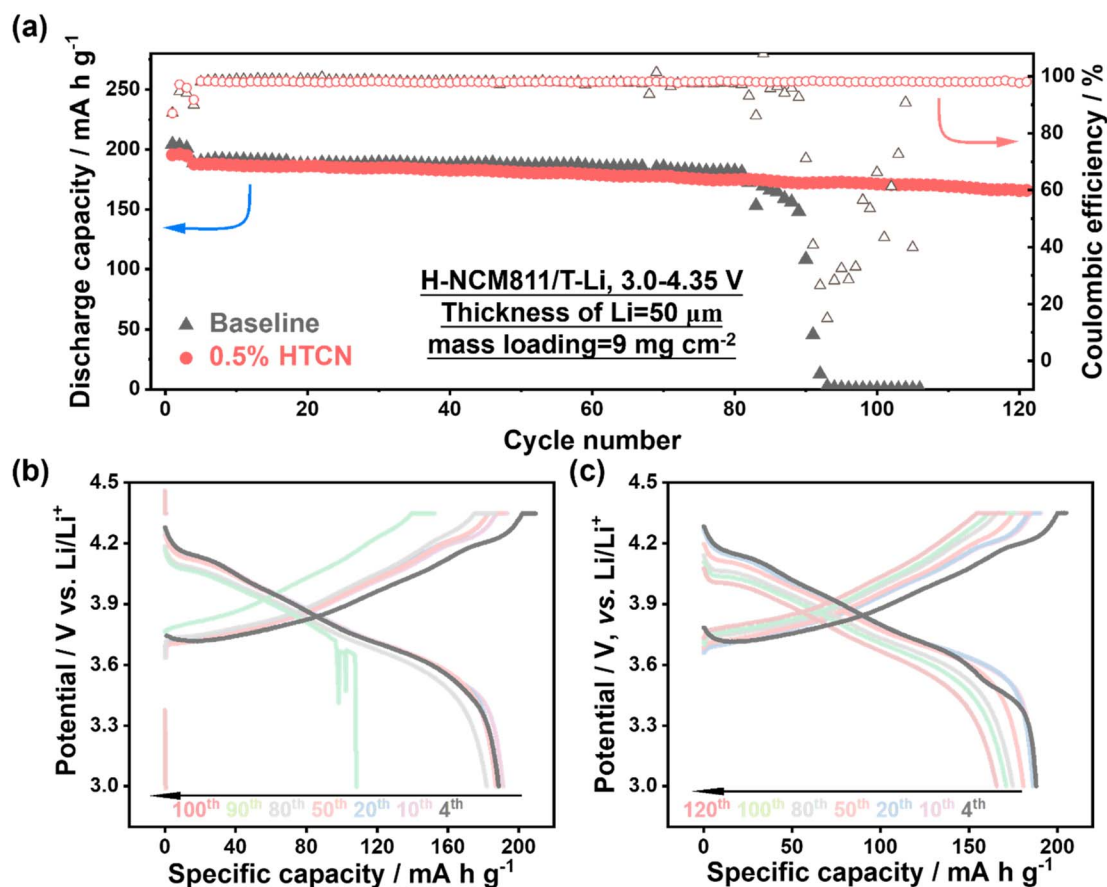

Fig. 6 (a) Cycling stability of H-NCM811//L-Li full cells in various electrolytes at 0.2C for the initial three cycles and 1C for the subsequent cycles. Selected charge/discharge curves cycled in (b) baseline and (c) HTCN-containing electrolytes.

products of the electrolyte, and the primary particles can no longer be visible (Fig. S23a†). Meanwhile, a thick dead Li layer (Fig. S24a and b†) can be observed in baseline electrolytes, which seriously threatens the safety of the battery. In contrast, a relatively clean surface of the NCM811 cathode (Fig. S23b†) and a thinner SEI film with a thickness of 16.2 μm on the Li anode (Fig. S24c and d†) are observed in the electrolyte with the HTCN additive. These results further prove the potency of the HTCN additive to improve interface compatibility.

4. Conclusions

In this work, we developed a novel nitrile additive, 1,3,6-hexanetricarbonitrile (HTCN), in a carbonate electrolyte, which largely improves the overall electrochemical performance of NCM811//Li full batteries. Theoretical calculations show that HTCN has stronger binding energy with transition metal ions and is more easily adsorbed on the cathode surface, where it is oxidized, compared with the carbonate solvent, involving the detachment of the CN group in the linear chain and the repolymerization of F^-. In addition, HTCN has a more negative electron affinity and is easier to reduce resulting from the detachment of the CN group in the side chain and the participation of the PF_6^- anion in the polymerization. Electrochemical tests and physical characterization further demonstrate that the HTCN additive preferentially oxidizes on the surface of the NCM811 cathode to construct a stable CEI film, while reducing on the Li metal anode surface to construct a robust SEI film. More importantly, HTCN can not only preferentially bind to PF_6^- thus inhibiting its thermal decomposition, but also combine with F^- to reduce the corrosion of HF on cathode materials. Therefore, the HTCN additive can not only significantly improve the cycle stability of the NCM811 cathode//Li anode full battery with a specific discharge capacity of 175 mA h g^{-1} after 120 cycles, but also realize a desired energy density of ~330 W h kg^{-1} at the cell level. Our work provides new insights into the development of new multifunctional additives.

Data availability

All the data supporting this article have been included in the main text and the ESI.†

Author contributions

The manuscript was written through contributions of all authors. All authors have given approval to the final version of the manuscript.

Conflicts of interest

There are no conflicts to declare.

Acknowledgements

References

1 W. Xu, J. L. Wang, F. Ding, X. L. Chen, E. Nasybutin, Y. H. Zhang and J. G. Zhang, *Energy Environ. Sci.*, 2018, 7, 513–537.

2 D. Lin, Y. Liu and Y. Cui, *Nat. Nanotechnol.*, 2017, **12**, 194–206.

3 H. Zhuang, H. Xiao, T. Zhang, F. Zhang, P. Han, M. Xu, W. Dai, J. Jiao, L. Jiang and Q. Gao, *Angew. Chem. Int. Ed.*, 2024, **63**, e202407315.

4 J. Liu, H. Hua, J. Lin, Y. Deng, N. Pei, P. Zhang, J. C. Dong, J. F. Li and J. Zhao, *Energy Environ. Sci.*, 2024, **17**, 5993–6002.

5 Y. Wang, M. Li, F. Yang, J. Mao and Z. Guo, *Energy Mater. Devices*, 2023, **1**, 9370005.

6 Y. Wang, X. Yang, Y. Meng, Z. Wen, R. Han, X. Hu, B. Sun, F. Kang, B. Li, D. Zhou, C. Wang and G. Wang, *Chem. Rev.*, 2024, **124**, 3494–3589.

7 T. D. Pham, A. Bin Faheem, J. Kim, H. M. Oh and K. K. Lee, *Small*, 2022, **18**, 1–15.

8 Z. Peng, X. Cao, P. Gao, H. Jia, X. Ren, S. Roy, Z. Li, Y. Zhu, W. Xie, D. Liu, Q. Li, D. Wang, W. Xu and J. G. Zhang, *Adv. Funct. Mater.*, 2020, **30**, 1–13.

9 K. Zhang, J. Chen, W. Feng, C. Wang, Y. N. Zhou and Y. Xia, *J. Power Sources*, 2023, **553**, 232311.

10 H. Zhang, Z. Zeng, F. Ma, Q. Wu, X. Wang, S. Cheng and J. Xie, *Angew. Chem. Int. Ed.*, 2023, **62**, e202300771.

11 S. Zhang, J. F. Ding, R. Xu, Y. Xiao, C. Yan and J. Q. Huang, *Adv. Energy Mater.*, 2024, **14**, 2303726.

12 J. Liu, X. Li, J. Huang, G. Yang and J. Ma, *Adv. Funct. Mater.*, 2024, **34**, 2312762.

13 R. He, K. Deng, D. Mo, X. Guan, Y. Hu, K. Yang, Z. Yan and H. Xie, *Angew. Chem. Int. Ed.*, 2024, **63**, e202317176.

14 B. Liao, X. Hu, M. Xu, H. Li, L. Yu, W. Fan, L. Xing, Y. Liao and W. Li, *J. Phys. Chem. Lett.*, 2018, **9**, 3434–3445.

15 K. Jung and T. Yim, *J. Alloys Compd.*, 2020, **834**, 155155.

16 Y. Jin, T. Zhang and M. Zhang, *Adv. Energy Mater.*, 2022, **12**, 1–20.

17 G. Li, Y. Liao, Z. Li, N. Xu, Y. Lu, G. Lan, G. Sun and W. Li, *ACS Appl. Mater. Interfaces*, 2020, **12**, 37013–37026.

18 L. Ding, Y. Chen, Y. Sheng, X. Yue and Z. Liang, *Angew. Chem. Int. Ed.*, 2024, **63**, e202411933.

19 C. X. Bi, N. Yao, X. Y. Li, Q. K. Zhang, X. Chen, X. Q. Zhang, B. Q. Li and J. Q. Huang, *Adv. Mater.*, 2024, **36**, 2411197.

20 W. Bao, R. Wang, C. Qian, H. Shen, F. Yu, H. Liu, C. Guo, J. Li and K. Sun, *Small*, 2024, **20**, 202307179.

21 Z. A. Ghazi, Z. Sun, C. Sun, F. Qi, B. An, F. Li and H. M. Cheng, *Small*, 2019, **15**, 1–26.

22 Q. Ma, J. Cui, J. Luo and A. Dong, *ACS Appl. Energy Mater.*, 2022, **5**, 3–13.

23 S. Liu, Q. Zhang, X. Wang, M. Xu, W. Li and B. L. Lucht, *ACS Appl. Mater. Interfaces*, 2020, **12**, 33719–33728.

24 J. Wu, Z. Gao, Y. Wang, X. Yang, Q. Liu, D. Zhou, X. Wang, F. Kang and B. Li, *Nano–Micro Lett.*, 2022, **14**, 1–13.

25 T. Li, K. Chen, B. Yang, K. Li, B. Li, M. He, L. Yang, A. Hu and J. Long, *Chem. Sci.*, 2024, **15**, 12108–12117.

26 J. Shi, T. Koketsu, Z. Zhu, M. Yang, L. Sui, J. Liu, M. Tang, Z. Deng, M. Liao, J. Xiang, Y. Shen, L. Qie, Y. Huang, P. Strasser and J. Ma, *Nat. Mater.*, 2024, **23**, 1686–1694.

27 Y. H. T. Tran, K. An, D. T. T. Vu and S. W. Song, *ACS Energy Lett.*, 2025, **10**, 356–370.

28 W. H. Hou, Y. Ou, T. Zeng, Q. Feng, Q. Cao, P. Zhou, Y. Xia, X. Song, W. Zhang, Y. Lu, S. Yan, H. Y. Zhou, H. Zhou, H. Liu, F. Liu and K. Liu, *Energy Environ. Sci.*, 2024, **17**, 8325–8336.

29 Y. Lu, Q. Cao, W. Zhang, T. Zeng, Y. Ou, S. Yan, H. Liu, X. Song, H. Zhou, W. Hou, P. Zhou, N. Hu, Q. Feng, Y. Li and K. Liu, *Nat. Energy*, 2024, **10**, 356–370.

30 Y. Chen, S. L. Liao, H. Gong, Z. Zhang, Z. Huang, S. C. Kim, E. Zhang, H. Lyu, W. Yu, Y. Lin, P. Sayavong, Y. Cui, J. Qin and Z. Bao, *Chem. Sci.*, 2024, **15**, 19805–19819.

31 S. Li, Z. Luo, H. Tu, H. Zhang, W. Deng, G. Zou, H. Hou and X. Ji, *Energy Storage Mater.*, 2021, **42**, 679–686.

32 S. Li, Z. Luo, L. Li, J. Hu, G. Zou, H. Hou and X. Ji, *Energy Storage Mater.*, 2020, **32**, 306–319.

33 Y. Cui, C. Yang, Z. Zhuang, M. Wang and Q. Zhuang, *J. Inorg. Organomet. Polym. Mater.*, 2018, **28**, 731–737.

34 J. F. Ding, R. Xu, N. Yao, X. Chen, Y. Xiao, Y. X. Yao, C. Yan, J. Xie and J. Q. Huang, *Angew. Chem. Int. Ed.*, 2021, **60**, 11442–11447.

35 Y. Gao, G. Wu, W. Fang, Z. Qin, T. Zhang, J. Yan, Y. Zhong, N. Zhang and G. Chen, *Angew. Chem. Int. Ed.*, 2024, **63**, e202403668.

36 J. Jiang, M. Li, X. Liu, J. Yi, Y. Jiang, C. Wu, H. Liu, B. Zhao, W. Li, X. Sun, J. Zhang and S. Dou, *Adv. Energy Mater.*, 2024, **14**, 2400365.

37 S. H. Lee, J. Y. Hwang, S. J. Park, G. T. Park and Y. K. Sun, *Adv. Funct. Mater.*, 2019, **29**, 1–9.

38 Y. Qiu, D. Lu, Y. Gai and Y. Cai, *ACS Appl. Mater. Interfaces*, 2022, **14**, 11398–11407.

39 T. Zhou, J. Wang, L. Lv, R. Li, L. Chen, S. Zhang, H. Zhang, B. Ma, J. Huang, B. Wu, L. Chen, T. Deng and X. Fan, *Energy Environ. Sci.*, 2024, **40**, 16669–16680.

40 Y. Xu, L. Wan, J. Liu, L. Zeng and Z. Yang, *J. Alloys Compd.*, 2017, **698**, 207–214.

41 S. Brox, S. Röser, T. Husch, S. Hildebrand, O. Fromm, M. Korth, M. Winter and I. Cekic-Laskovic, *ChemSusChem*, 2016, **9**, 1704–1711.

42 Y. Abu-Lebdeh and I. Davidson, *J. Power Sources*, 2009, **189**, 576–579.

43 P. He, M. Zhang, J. Wu, Y. Li, Y. Wang, Y. Yan, D. Zhang and X. Sun, *J. Alloys Compd.*, 2023, **967**, 171822.

44 Y. Chen, D. Liu, X. Xu, X. Wang, X. X. Jiao, Y. Bai, S. Xiong, A. S. Vasenko, Y. Wang, Z. Song and Y. Liu, *Small Methods*, 2024, **8**, 2401178.

45 Y. Zhang, N. Yao, X. Tang, H. Wang, M. Zhang, Z. Wang, A. Shao, J. Liu, L. Cheng, Y. Guo and Y. Ma, *Adv. Energy Mater.*, 2024, **14**, 2402918.

46 H. Yang, G. V. Zhuang and P. N. Ross, *J. Power Sources*, 2006, **161**, 573–579.

47 M. Dixit, B. Markovsky, F. Schipper, D. Aurbach and D. T. Major, *J. Phys. Chem. C*, 2017, **121**, 22628–22636.

48 X. Liu, G. L. Xu, L. Yin, I. Hwang, Y. Li, L. Lu, W. Xu, X. Zhang, Y. Chen, Y. Ren, C. J. Sun, Z. Chen, M. Ouyang and K. Amine, *J. Am. Chem. Soc.*, 2020, **142**, 19745–19753.